ELSEVIER

Journal of Crystal Growth 165 (1996) 137–146

JOURNAL OF CRYSTAL GROWTH

# Stability of double-diffusive convection in a freckle-free solidification system

Jay W. Lu, Falin Chen *

*Institute of Applied Mechanics, National Taiwan University, Taipei 10764, Taiwan, ROC*

Received 30 August 1995; accepted 25 October 1995

**Abstract**

The stability of the double-diffusive convection of a binary solution unidirectionally solidified from above, a freckle-free system, is investigated analytically. Results show that, interestingly, the stability characteristics of the double-diffusive convection resemble those of thermal convection in a similar system. This conclusion is reached on the basis of the following results: First, the neutral curve is invariably uni-modal. Secondly, the critical Rayleigh number increases linearly with the viscosity contrast coefficient $\gamma$ (defined in Eq. (14)). Thirdly, the onset of convection is confined to the region below a stagnant lid of thickness $\ln \gamma^*$ (defined in Section 5.3). Finally, the stability characteristics of the convection are significantly influenced by the viscosity variation, the Prandtl number, and the temperature of bulk fluid, the three parameters influential on the thermal boundary layer thickness; other physical parameters, such as the Darcy number of the mushy zone, the concentration ratio, and the Stefan number, corresponding with the variation of the morphology of the mush, have relatively insignificant effect on the stability of convection. All the above four facets also hold for the thermal convection of the system in which a pure fluid is solidified from above. This resemblance explains why the present cooling-from-above system is freckle-free.

## 1. Introduction

In developing the advanced metal for the turbine blades of aircraft engine, the so-called unidirectional solidification process technique is extensively employed. In the process, the alloy melt is solidified by cooling from *below* of the mould. The resultant casting shows increased creep rupture strain as well as improved thermal fatigue behavior, two most important features for the modern turbine blades. Under some circumstances, however, defects are present, causing deleterious effect on the mechanical properties of the casting. The defects are knows as freckles, which contain solute-rich, eutectic structure alloy in columnar regions extending longitudinally in the direction of solidification [1,2]. To investigate the occurrence of freckles, an analogous system using an aqueous ammonium chloride solution cooled from below is frequently considered. In such a system, it was observed that isolated plumes of depleted buoyant fluid issue directly from the interior of the dendritic mushy zone [3–10], which is not unlike the freckles in the alloy castings. The occurrence of the plume is believed to be induced by a subcritical instability of the convection under the strong perturbation of the nonlinear salt-finger convection [11–13], a double-diffusive convection prevailing above

* Corresponding author.


*PII* S0022-0248(96)00146-7

the dendritic mushy zone. The stability of the salt-finger convection, accordingly, is closely related to the plume convection.

In the present paper, we propose a freckle-free system in which the melt is unidirectionally solidified from *above*. For such a system, the resultant casting preserves the superiority which the casting of cooling-from-below system holds, while the formation of freckles has never been observed [14]. The double-diffusive convection occurred in the cooling-from-above system, accordingly, should be responsible for the plume-free result. We thus study the stability characteristics of this convective flow, in a hope to obtain a better understanding of the mechanism driving the formation of freckles.

It is known that in the case of cooling-from-below, the double-diffusive convection is of salt-finger type since the thermal gradient is a stabilizing factor and the solutal gradient is a destabilizing factor [15]. In the case of cooling-from-above, however, the double-diffusive convection is of diffusive type in which the two gradients now play opposite roles. So far, the research effort made for the convection in the cooling-from-above system has not been so much as that made for the cooling-from-below system because the unsteady nature of the diffusive-type convection increases both the physical complexity as well as the numerical difficulty. Theoretically, Hurle, Jakeman and Wheeler [16] investigated the convective instability of a binary alloy solidifying from above, in which the melt and the solid was divided by a sharp interface. Smith [17] investigated the onset of thermal convection during the solidification of a pure fluid with temperature-dependent viscosity. He found that for large viscosity contrast between cold and hot regions, the critical Rayleigh number increases linearly with a parameter accounting for the contrast of viscosity, and the onset of convection is largely confined to the region below a stagnant lid in which no convection occurs. Experimentally, Kerr et al. [18–20] in three consecutive papers studied the interaction between the solidification and the convection when a binary solution solidified from above. Since emphasis was placed on the crystallization and the composition variation in the solid, no detail of the stability characteristics of the convection was reported.

As mentioned above, none of these studies was devoted to studying the stability of the double-diffusive convection in a binary solution unidirectionally solidified from above, which we investigate in the present paper. In so doing, we have one thing in mind, that the plume-free (or freckle-free) system may be applied to the manufacturing of single-crystal turbine blade, which under the conventional cooling-from-below system has been long suffering from the formation of freckles. We nevertheless note that many other castings are also manufactured by cooling from above, which the present analysis may apply to as well. We first demonstrate the mathematical formulation in Section 2. Based on this formulation, the motionless basic state solution is obtained in Section 3. Then the linearized small disturbance equations are shown in Section 4. In Section 5, the stability characteristics of the double-diffusive flow under the influence of several varying physical parameters are discussed. In particular, the influence of the viscosity variation is illustrated since the variable viscosity effect can be significant in the metallic system when the temperature decreases from working condition to melting point. In Section 6 a conclusion is provided.

## 2. Mathematical formulation

Consider a hypereutectic binary solution of concentration $C_\infty$ ($> C_E$) and temperature $T_\infty$ unidirectionally solidifying from above, where $C_E$ is the eutectic concentration of the solution. As a result of the morphological instability of the eutectic front, a dendritic mushy region forms below the eutectic solid region and above a semi-infinite fluid region (Fig. 1). The mushy layer extends from $z = 0$ to $z = h$. The position of the melt/mush interface is to be determined as part of the solution. Both the solid/mush and the mush/fluid interfaces are assumed moving downwards with a constant velocity $V$. The temperature at the mush/solid interface is fixed at the eutectic temperature $T_E$. Since hypereutectic alloy is considered and that the fluid density increases with $C_\infty$ is assumed, the ejected fluid in the vicinity of the mush/fluid interface can be of less concentrated and of lower temperature than the bulk fluid, and a double-diffusive convection may occur. We study the stability of this convection.

Two sets of equations are required to describe the fluid motion of the system. Each set consists of the conservation of mass, momentum, heat, and solute. The density of the fluid is assumed to be constant except in the gravity term, in which the density is a function of temperature and concentration. The viscosity of the fluid is considered as a function of temperature

$$\mu^* = \mu_0 \exp[-c(T - T_\infty)], \tag{1}$$

where $c > 0$ is an arbitrary constant, $\mu_0 = \nu_0 \rho_0$ is the reference dynamic viscosity, and $\nu_0$ and $\rho_0$ are reference kinematic viscosity and reference density, respectively. Eq. (1) indicates that the viscosity of the fluid decreases with increasing temperature, which is relevant to most of the Newtonian fluids as well as the liquid metals. We nondimensionalize the fluid velocities with the interface velocity $V$, distances with $\kappa_{tl}/V$, time with $\kappa_{tl}/V^2$, and pressure with $\beta \Delta C \rho_0 g \kappa_{tl}/V$; in which $\kappa_{tl}$ is the thermal diffusivity of the fluid, $\beta = \beta^* - \Gamma\alpha^*$, $\beta^*$ and $\alpha^*$ are solutal and thermal expansion coefficients, respectively, $\Gamma$ is the slope of the liquidus curve, which is assumed to be constant, $\Delta C = C_\infty - C_E$, and $g$ is the gravitational acceleration. By assuming the physical properties of the fluid and solid to be identical and by taking the Galilean transformation with respect to the moving interface, we obtain the following dimensionless equations. In the fluid region $h < z < \infty$, we have

$$\nabla \cdot \boldsymbol{u} = 0, \tag{2}$$

$$\left(\frac{\partial}{\partial t} - \frac{\partial}{\partial z}\right)\theta + \boldsymbol{u} \cdot \nabla\theta = \nabla^2\theta, \tag{3}$$

$$\left(\frac{\partial}{\partial t} - \frac{\partial}{\partial z}\right)\Theta + \boldsymbol{u} \cdot \nabla\Theta = \epsilon\nabla^2\Theta, \tag{4}$$

$$\frac{1}{\sigma}\left[\left(\frac{\partial}{\partial t} - \frac{\partial}{\partial z}\right) + \boldsymbol{u} \cdot \nabla\right]\boldsymbol{u} = \nabla \cdot (\mu \boldsymbol{D}) - R_T \theta \boldsymbol{e}_k + R_C\left(\Theta \boldsymbol{e}_k - \frac{\beta}{\beta^*}\nabla p\right), \tag{5}$$

where $\boldsymbol{u} = (u, v, w)$ is the velocity vector in the Cartesian coordinate, $\boldsymbol{D} = \nabla\boldsymbol{u} + \nabla\boldsymbol{u}^T$ is the deviatoric strain tensor and T denotes the transverse of the tensor, the dimensionless temperature and concentration are defined as

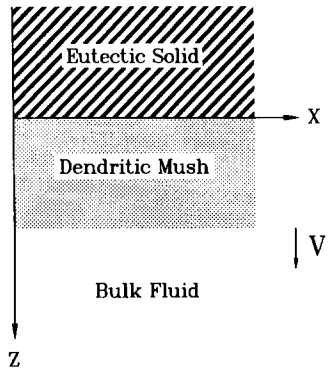


Fig. 1. Schematic description of the physcial domain considered. The mushy-layer height is $h$.

$$\theta = \frac{T - T_L(C_\infty)}{\Delta T}, \quad \Theta = \frac{C - C_\infty}{\Delta C}, \tag{6}$$

where $\Delta T = \Gamma \Delta C = T_L(C_\infty) - T_E$, $T_L(C_\infty)$ is the liquidus temperature corresponding to $C_\infty$, $\epsilon = \kappa_{cl}/\kappa_{tl}$ is the Lewis number, $\kappa_{cl}$ is the solutal diffusivity of the fluid, $\sigma = \nu/\kappa_{tl}$ is the Prandtl number, $e_k$ is the unit vector in the vertical direction, $p$ is the pressure, $R_T$ and $R_C$ are thermal and solutal Rayleigh numbers given by

$$R_T = \frac{g\alpha^* \Delta T H^3}{\kappa_{tl}\nu_0}, \quad R_C = \frac{g\beta^* \Delta C H^3}{\kappa_{tl}\nu_0}, \tag{7}$$

in which $H = \kappa_{tl}/V$ is the characteristic length. In the mushy region $0 < z < h$, we have

$$\nabla \cdot \boldsymbol{u} = 0, \tag{8}$$

$$\left(\frac{\partial}{\partial t} - \frac{\partial}{\partial z}\right)\theta + \boldsymbol{u} \cdot \nabla\theta = \nabla^2\theta - \mathscr{F}\left(\frac{\partial}{\partial t} - \frac{\partial}{\partial z}\right)\chi, \tag{9}$$

$$\chi\left(\frac{\partial}{\partial t} - \frac{\partial}{\partial z}\right)\Theta + \boldsymbol{u} \cdot \nabla\Theta = -(\Theta - C)\left(\frac{\partial}{\partial t} - \frac{\partial}{\partial z}\right)\chi, \tag{10}$$

$$\frac{\mu \boldsymbol{u}}{\Pi(\chi)} = R_m(-\nabla p + \theta \boldsymbol{e}_k), \tag{11}$$

where $\chi$ is the porosity, $\mathscr{C} = (C_S - C_\infty)/\Delta C$ is the concentration ratio and $C_S$ is the composition of the

solid phase, $\mathscr{F} = \mathscr{L}/c\Delta T$ is the Stefan number, $\mathscr{L}$ is the latent heat of fusion, $c$ is the specific heat, and the Rayleigh number for the mushy layer is given by

$$R_m = \frac{g\beta\Delta C\Pi_0 H}{\kappa_{tl}\nu_0}, \tag{12}$$

in which $\Pi_0$ is the reference permeability. The dimensionless viscosity function $\mu$ is defined as

$$\mu = \exp\left[\gamma\frac{\theta_\infty - \theta_b}{\theta_\infty - \theta_E}\right], \tag{13}$$

where

$$\gamma = \ln\left[\frac{\mu_E}{\mu_\infty}\right], \tag{14}$$

accounting for the viscosity contrast between the fluid at the eutectic front and the bulk fluid, and $\theta_b$ is the dimensionless basic state temperature to be shown in Section 3. The dimensionless permeability function $\Pi(\chi)$ is an arbitrary function of the porosity $\chi$, which is assumed to be uniform as $\Pi(\chi) = 1$ for the present study. The assumption of uniform permeability actually is supported by the analysis of Chen et al. [13] that the stability criteria of a similar flow using $\Pi(\chi) = 1$ are in good agreement with the experimental results. Note that since the thermodynamic equilibrium condition holds in the mushy layer [13], the liquidus relation $\theta = \Theta$ is applied in the mushy layer. Note also that since the solute diffusion in the mush is so small, we assume $\epsilon$ in the mush to be zero, which is justified by the previous studies [11,13].

The boundary conditions at $z \to \infty$ are

$$\theta \to \theta_\infty, \quad \Theta \to 0, \quad \boldsymbol{u} \to \boldsymbol{0}, \tag{15a–15c}$$

at the melt/mush interface $z = h$ are

$$\theta = \Theta, \quad \boldsymbol{n}\cdot\nabla\theta = \boldsymbol{n}\cdot\nabla\Theta, \quad [\boldsymbol{n}\cdot\boldsymbol{u}] = 0,$$

$$[\theta] = 0, \quad [\boldsymbol{n}\cdot\nabla\theta] = 0, \quad \chi = 1, \quad [\sigma_n] = 0,$$

$$\left.\frac{\partial \boldsymbol{u}_2}{\partial z}\right|_{h+} = \Lambda\sqrt{\frac{\mathscr{H}}{\Pi(1)}}\left(\boldsymbol{u}_2|_{h+} - \boldsymbol{u}_2|_{h-}\right), \tag{16a–16h}$$

where the square brackets denote the jump of the enclosed quantity across the interface, $\boldsymbol{n}$ is a unit vector normal to the interface, $\boldsymbol{u}_2$ is the plane velocity vector $(u,v)$, and $\sigma_n$ is the normal stress on the interface. In above boundary conditions, Eq. (16a) is the liquidus relation applying at the interface, Eq. (16b) is the marginal equilibrium condition [21], Eq. (16c) is the continuity of normal velocity, Eqs. (16d) and (16e) are continuities of temperature and heat flux, respectively, Eq. (16f) is an enforced condition assuming the solid at the interface vanishes, Eq. (16g) is the continuity of normal stress, and Eq. (16h) is the Beavers–Joseph boundary condition illustrating that the normal gradient of the horizontal velocity above the melt/mush interface is proportional to the difference between the horizontal velocities above and below the interface [22], and $\mathscr{H} = H^2/\Pi_0$. The condition Eq. (16f) holds under the assumptions that the interface is a perfect flat plane and the solid at the tip of the dendrite virtually vanishes. At the mush/solid interface $z = 0$ we have

$$\theta = -1, \quad w = 0. \tag{17a–17b}$$

## 3. Basic state solution

The equations and associated boundary conditions of Section 2 admit a steady solution in terms of a function of $z$. In the fluid layer, as $\boldsymbol{u}$ vanishes, Eqs. (3) and (4) become respectively

$$-\theta_b' = \theta_b'', \tag{18}$$

$$-\Theta_b' = \epsilon\Theta_b'', \tag{19}$$

where the index b accounts for the basic state of the melt region. Along with the relevant boundary conditions, the basic state temperature and concentration can be obtained as

$$\theta_b = \theta_\infty + (\theta_i - \theta_\infty)\,e^{-(z-h)}, \tag{20}$$

$$\Theta_b = \theta_i\,e^{-(z-h)/\epsilon}, \tag{21}$$

with the interfacial temperature given by

$$\theta_i = -\frac{\epsilon}{1-\epsilon}\theta_\infty. \tag{22}$$

In the mushy layer, the relation $\theta = \Theta$ applies. From Eqs. (9) and (10), one can obtain the basic state equations of the mushy region as

$$-\theta_{bm}' = \theta_{bm}'' + \mathscr{F}\chi_b', \tag{23}$$

$$-\chi_b\theta_{bm}' = (\theta_{bm} - \mathscr{C})\chi_b'. \tag{24}$$

By integrating Eqs. (23) and (24) from $z$ to $h$ and by applying associated boundary conditions, we can obtain the following relations

$$\chi_b = \frac{\mathscr{C} - \theta_i}{\mathscr{C} - \theta_{bm}}, \tag{25}$$

$$z = \frac{A - \mathscr{C}}{A - B}\ln\left(\frac{A+1}{A-\theta_b}\right) + \frac{\mathscr{C} - B}{A - B}\ln\left(\frac{B+1}{B-\theta_b}\right), \tag{26}$$

where $A = A_1 + B_1$, $B = A_1 - B_1$, $A_1 = (\mathscr{C} + \theta_\infty + \mathscr{F})/2$, and $B_1^2 = A_1^2 - \mathscr{C}\theta_\infty - \mathscr{F}\theta_i$. Eqs. (23) to (26) are solved numerically.

## 4. Small disturbance equations

We linearize the equations of Section 2 by introducing small disturbances to the basic state quantities of Section 3 and by substituting their combination into the original equations. After obtaining the linearized equations by neglecting higher-order terms of disturbance quantities and introducing the normal modes proportional to $e^{\omega t + i\alpha\chi}$, the small disturbance equations are as follows. In the fluid layer, we have

$$(D^2 - \alpha^2)W = \Omega, \tag{27}$$

$$[D^2 + D - \omega - \alpha^2]\theta = \theta_b' W, \tag{28}$$

$$[\epsilon D^2 + D - \omega - \epsilon\alpha^2]\Theta = \Theta_b' W, \tag{29}$$

$$\left[\mu(D^2 - \alpha^2) + \frac{D-\omega}{\sigma} + 2\mu' D\right]\Omega + \mu''(\Omega + 2\alpha^2 W) = -\alpha^2[R_T\theta + R_C\Theta]. \tag{30}$$

In these equations, the notations $W$, $\theta$, $\Theta$ now represent small disturbance quantities. In addition, both $'$ and $D$ represent the vertical derivative $\mathrm{d}/\mathrm{d}z$, $\alpha$ is the horizontal wave number, $\omega$ is the normal mode frequency, and $\Omega$ is the disturbance vorticity. Note that the Rayleigh numbers in the fluid can be replaced by the Rayleigh number in the mush by the relations $R_T = \mathscr{A}\mathscr{H}R_m$ and $R_C = (1 + \mathscr{A})\mathscr{H}R_m$, where $\mathscr{A} = \Gamma\alpha^*/\beta$ is the buoyancy ratio between the buoyancy due to temperature to that due to concentration.

Similarly, in the mushy layer we have

$$(D^2 + D - \omega - \alpha^2)\theta + \mathscr{F}(D - \omega)\chi = \theta_b' W, \tag{31}$$

$$[\chi_b(D - \omega) + \chi_b']\theta + [(\theta_b - \mathscr{C})(D - \omega) + \theta_b']\chi = \theta_b' w, \tag{32}$$

$$[f(D^2 - \alpha^2) + f'D]W = -\alpha^2 R_m\theta, \tag{33}$$

where $f = \mu/\Pi(\chi_b)$. Note that in Eq. (32) the liquidus relation $\theta = \Theta$ has been applied.

The boundary conditions at $z \to \infty$ are

$$\theta = 0, \quad \Theta = 0, \quad W = 0, \quad DW = 0, \tag{34a–34d}$$

at $z = h$ are

$$\theta = \Theta, \quad D\Theta - D\theta = \left(\frac{1-\epsilon}{\epsilon}\right)\theta_b'\eta, \quad [W] = 0,$$

$$[\theta] = 0, \quad [D\theta] = -\frac{\mathscr{F}\theta_b'}{\mathscr{C} - \theta_i}\eta, \quad \chi = \frac{\theta_b'}{\theta_i - C}\eta,$$

$$DW|_{h-} = -\frac{\Pi(1)}{\mathscr{H}\mu}\left[-\frac{1}{\sigma}(\omega - D)DW + \mu'(D^2 + \alpha^2)W + \mu D\Omega - 2\mu\alpha^2 DW\right]_{h+},$$

$$D^2 W|_{h+} = \Lambda\sqrt{\frac{\mathscr{H}}{\Pi(1)}}\,(DW|_{h+} - DW|_{h-}) \tag{35a–h}$$

and at $z = 0$ are

$$\theta = 0, \quad W = 0, \tag{36a–b}$$

where $\eta$ is the small perturbation of the interface position.

Eqs. (27) to (36) forms a complex eigenvalue problem

$$F(R_m, \alpha, \omega; \theta_\infty, \mathscr{C}, \mathscr{A}, \epsilon, \sigma, \mathscr{F}, \mathscr{H}, \gamma) = 0 \tag{37}$$

having totally 13 orders of equation along with 14 boundary conditions, in which Eq. (35b) is employed to solve the disturbance melt/mush interface position $\eta$. We solve this complex eigenvalue problem with a shooting method. For the details of the numerical scheme the reader is referred to Chen et al. [13].

## 5. Results and discussion

Since no special alloy is preferred for the present analysis, the analogous aqueous solution system is considered. The relevant parameters are chosen as $\mathscr{C} = \mathscr{T} = \theta_\infty = 1$, $\sigma = 10$, $\epsilon = 0.025$, $\mathscr{A} = 0.5$, $\mathscr{H} = 10^5$, $\gamma = 0$, and the permeability is uniform $\Pi(\chi) = 1$; which to some extent are able to account for the physical properties of an aqueous solutions solidified under the experimental conditions of a laboratory. As we consider the variable viscosity effect ($\gamma > 0$), the viscosity is a function of temperature as shown in Eq. (13). The effects of the parameters $\mathscr{A}$, $\gamma$, $\sigma$, $\theta_\infty$, $\mathscr{H}$, $\mathscr{C}$, and $\mathscr{T}$, are studied. As one considers the effect of one parameter, the values of the other parameters are fixed as shown above.

### 5.1. Nature of the stability

For the present system, a supereutectic solution solidifying from above, the thermal gradient is destabilizing the fluid while the solutal gradient is stabilizing, which may result in a diffusive-type double-diffusive convection and in a large parameter range the convection can be oscillatory in nature [23]. However, for all the cases considered in the present study, the onset of convection is found to be invariably steady (i.e. $\omega \equiv 0$) and the neutral curve is in general uni-modal, i.e. only one minimum for a neutral curve. This is due to the fact that the onset of convection is of the length scale of the thermal boundary layer in the fluid region while the solutal boundary layer thickness is relatively so small that it plays virtually no role in determining the stability characteristics of the onset flow. In other words, the stability characteristics of the present double-diffusive convection are dominated by the thermal gradient, which will be shown in subsequent subsections.

### 5.2. $\mathscr{A}$ effect

The buoyancy ratio $\mathscr{A}$ is the ratio between the buoyancy due to temperature to that due to concentration, accounting in essence for the interaction between thermal and concentration gradients (a double-diffusive effect). Fig. 2 demonstrates the neutral curves represented by the three Rayleigh numbers $R_C$, $R_T$ and $R_m$ versus $\alpha$. Fig. 2a shows that the

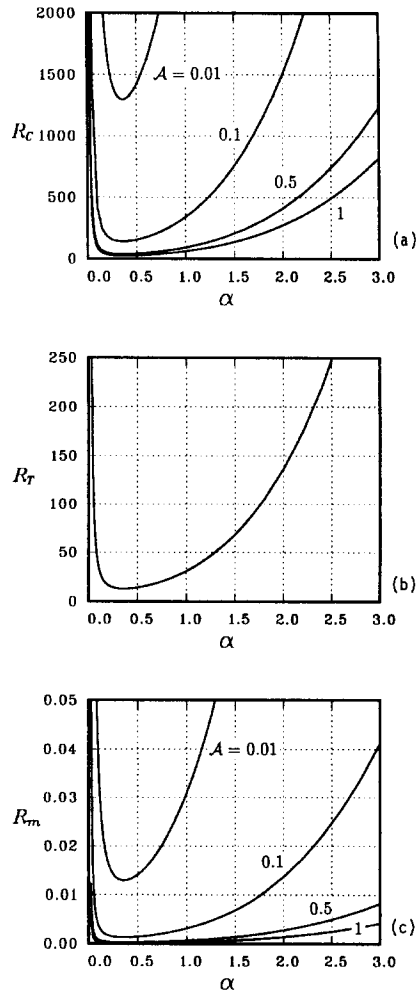


Fig. 2. Neutral curves for various $\mathscr{A}$. (a) $R_C$ versus $\alpha$; (b) $R_T$ versus $\alpha$; (c) $R_m$ versus $\alpha$.

critical $R_C$ (the minimum of $R_C$ of each curve) increases as $\mathscr{A}$ decreases, whereas Fig. 2b shows that the critical $R_T$ remains the same for different non-zero $\mathscr{A}$. The results of these two figures in fact can be related by the following relation

$$\frac{R_C}{R_T} = \frac{1}{\mathscr{A}} + 1 \tag{38}$$

for the non-zero $\mathscr{A}$. Since $R_T$ remains constant for varying $\mathscr{A}$, one can see from the relation $R_T = \mathscr{A}\mathscr{H}R_m$ that $R_m$ increases as $\mathscr{A}$ decreases (Fig. 2c); namely, the system is more stable for smaller $\mathscr{A}$. From the definition $\mathscr{A} = \Gamma\theta^*/\beta$, we see that smaller

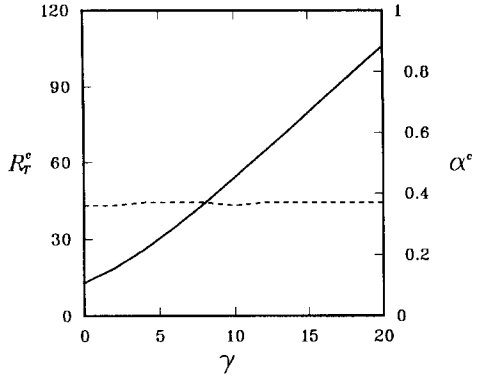


Fig. 3. The variations of $R_T^c$ (—) and $\alpha_c$ (---) versus $\gamma$.

$\mathscr{A}$ means lower thermal buoyancy and thus smaller destabilizing factor, leading to a more stable state. We nevertheless find that the onset streamline patterns for different $\mathscr{A}$ are virtually the same; in which the convection is largely confined to the fluid region and the fluid in the mush does not participate in the initial instability. This may be due to that the stability criteria in terms of $R_T$ is the same for different $\mathscr{A}$.

### 5.3. $\gamma$ effect

As shown in Eq. (14), $\gamma$ accounts for the viscosity contrast between the fluid at the eutectic front ($\gamma_E$) and the bulk fluid ($\gamma_\infty$). As $\gamma$ increases, the viscosity of the fluid near the eutectic front (the mush/solid interface) increases if the bulk fluid viscosity at infinity is constant. As a result, the fluid becomes more stable as a whole (Fig. 3) and the onset of convection is confined to the fluid region under a stagnant lid of increasing thickness (Fig. 4), which is in accord with the observation of Smith [17] who considered a single component fluid solidifying from above. Note that in Fig. 4 the dashed line represents the melt/mush interface and the horizontal dimension is scaled on the basis of the height of the mushy layer.

Fig. 3 shows interestingly that the $R_T^c$ increases virtually linearly with $\gamma$ except in the range of small $\gamma$. This linear relation also holds in both the configuration of Smith [17] and a single component fluid layer heated from below [24]. This linearity can be explained with a proper rescaling of the problem by focusing on the local behavior of the instability, as shown in the following. Consider an appropriate definition of a local Rayleigh number

$$R_{\mathrm{loc}} = \frac{\alpha^* g \Delta T_{\mathrm{loc}} H^3}{\kappa \nu_{\mathrm{loc}}}, \tag{39}$$

where $\Delta T_{\mathrm{loc}} = T_\infty - T_b|_{z=z^*+h}$ is the temperature difference across the convection layer and $z^*$ is the thickness of the lid (see, for example, Fig. 4d). In terms of dimensionless temperature, the $\Delta T_{\mathrm{loc}}$ can be expressed as

$$\Delta T_{\mathrm{loc}} = \Delta T(\theta_\infty - \theta_i)\exp(-z^*). \tag{40}$$

Similarly, the viscosity at $z = z^* + h$ is

$$\nu|_{z=z^*+h} = \nu_{\mathrm{loc}} = \nu_\infty \exp(\gamma^* \mathrm{e}^{-z^*}), \tag{41}$$

which can be obtained by Eqs. (13) and (14) when $\gamma^* = \gamma(\theta_\infty - \theta_i)/(\theta_\infty - \theta_E)$ is applied. Accordingly, by substituting Eqs. (40) and (41) into Eq. (39) one can obtain

$$R_{\mathrm{loc}} = R_T(\theta_\infty - \theta_i)\exp(-z^* - \gamma^* \mathrm{e}^{-z^*}). \tag{42}$$

When the onset of convection occurs, it must first occur in the region below the stagnant lid with the

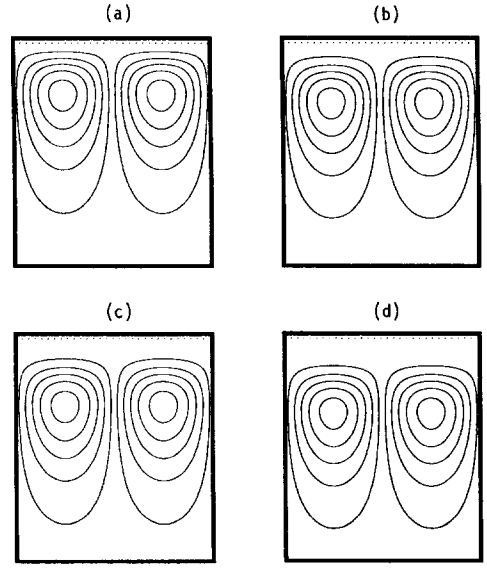


Fig. 4. The onset streamline patterns for various $\gamma$. The dotted line denotes the melt/mush interface, the top of the frame denotes the mush/solid interface, the wavelength is scaled with respect to the mush height. (a) $\gamma = 0$; (b) $\gamma = 5$; (c) $\gamma = 10$; (d) $\gamma = 20$.

largest possible $R_{loc}$, which must also be larger than a critical value for the onset of convection. The maximum value of $R_{loc}$ occurs at the position $z^* = z_{max}$, which can be obtained by $dR_{loc}/dz^* = 0$, yielding $z_{max} = \ln \gamma^*$. By substituting $z_{max}$ into Eq. (42), we obtain

$$R_{loc|max} = \frac{\theta_\infty - \theta_i}{e} \frac{R_T}{\gamma^*} \propto \frac{R_T}{\gamma^*}, \tag{43}$$

in which $(\theta_\infty - \theta_i)/e$ is a constant. Physically, this relation implies that the convection occurs in the region $\ln \gamma < z < \infty$ and the critical local Rayleigh number $R_{loc}$ is a constant; this is supported by the fact that the convection cells at onset are similar for all the cases of different $\gamma$ considered. As a result, according to Eq. (43) the value of $R_T^c$ of the system is linearly proportional to $\gamma^*$ (and $\gamma$ as well).

### 5.4. $\sigma$ effect

The Prandtl number $\sigma$ essentially accounts for the relative strength of advection to diffusion, as shown in Eq. (5). In the present moving reference frame due to the Galilean transformation, there is a basic vertical velocity toward the solidification front. The vorticity induced by buoyancy is advected by this velocity and is diffused as well. Accordingly, larger $\sigma$ tends to advect onset vorticity to the solidification front more than to diffuse away, enhancing the basic velocity and resulting in a less stable state. This scenario is supported by the numerical results shown in Fig. 5 that both $R_T^c$ and $\alpha^c$ decreases with increasing $\sigma$. As one can see from the previous results and

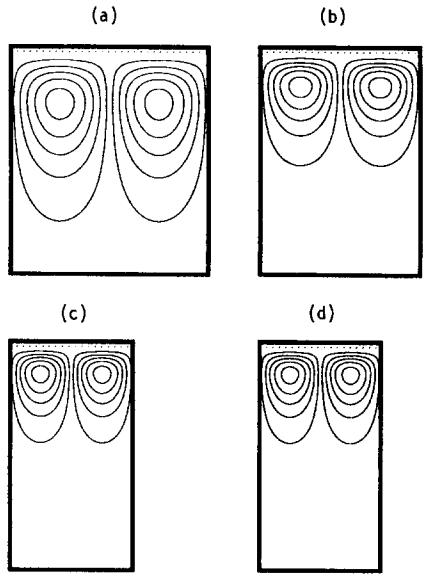


Fig. 6. The onset streamline patterns for various $\sigma$. (a) $\sigma = 10$; (b) $\sigma = 1$; (c) $\sigma = 0.1$; (d) $\sigma = 0.05$.

the results to be shown in subsequent subsections, the value of $\alpha^c$ is hardly influenced by the physical parameters except $\sigma$. This is because (Fig. 6) that the characteristics length of the convection cell is dominated by the thickness of the thermal boundary layer, which decreases with decreasing $\sigma$.

### 5.5. $\theta_\infty$ effect

The parameter $\theta_\infty$ represents the temperature of the bulk fluid, or equivalently the vertical thermal gradient in the system. Fig. 7 illustrates that $R_T^c$ decreases monotonically with increasing $\theta_\infty$ while $\alpha^c$

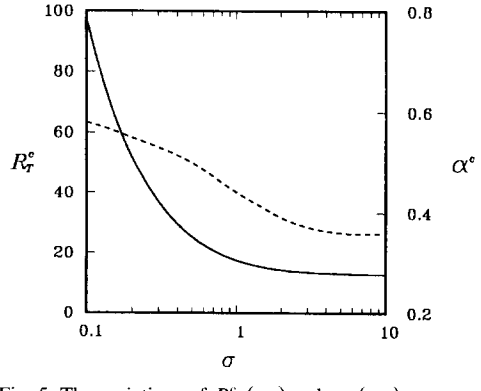


Fig. 5. The variations of $R_T^c$ (—) and $\alpha_c$ (---) versus $\gamma$.

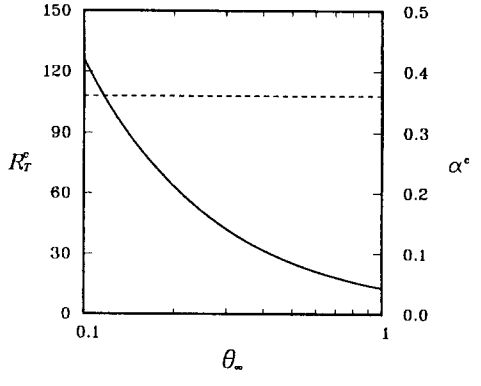


Fig. 7. The variations of $R_T^c$ (—) and $\alpha^c$ (---) versus $\theta_\infty$.

remains unchanged. Larger $\theta_\infty$ implies larger thermal gradient in the bulk fluid region so that a less stable state is induced. In addition, larger $\theta_\infty$ results in larger porosity and smaller mushy-layer height, both will lead to a less stable state for the system, while the latter factor is of much less significance.

### 5.6. $\mathscr{H}$ effect

The parameter $\mathscr{H}$, which by definition is equivalent to the inverse of Darcy number, measures the resistance to the flow in the mush. For the present problem, the onset of convection is largely confined to the fluid region and the fluid in the mush does not participate in the initial instability. The effect of $\mathscr{H}$ on the stability is therefore insignificant. As a result, both $R_T^c$ and $\alpha^c$ remains virtually unchanged as $\mathscr{H}$ varies from $10^4$ to $10^7$, although a slight increase of $R_T^c$ with $\mathscr{H}$ still can be observable because larger $\mathscr{H}$ implies smaller permeability, which in turn results in a more restricted environment to the flow in the mush and thus a more stable state.

### 5.7. $\mathscr{C}$ effect

The value of $\mathscr{C}$ primarily corresponds to the value of $C_\infty$. Larger $\mathscr{C}$ results in larger porosity of the mush and thus a less stable state of the system. The onset of convection, nevertheless, is again largely confined to the fluid region. The influence of $\mathscr{C}$ on the stability is accordingly not significant.

### 5.8. $\mathscr{F}$ effect

Larger Stefan number $\mathscr{F}$ implies less dissolution of the mush and thus a smaller porosity, the system is thus more stable for larger $\mathscr{F}$. However, again, the onset of convection occurs largely in the fluid region, and the influence of varying $\mathscr{F}$ on the stability is also insignificant.

## 6. Conclusion

We have proposed a freckle-free system in which a binary solution is unidirectionally solidified from above and have analyzed the stability of double-diffusive convection of the system. It is found that, for all the cases considered, the onset of convection is invariably steady in nature, despite the fact that the stabilizing solutal gradient and the destabilizing thermal gradient can lead to a diffusive-type (or overstable) convection, which is oscillatory in nature. This steady-onset convection is an outcome of the predominance of the thermal gradient in the bulk fluid region since the onset of convection is of the scale of thermal boundary layer thickness while the solutal boundary layer thickness is relatively so small that it primarily plays an insignificant role in determining the stability characteristics of the onset of convection.

As the viscosity is temperature dependent, the critical Rayleigh number $R_T^c$ increases linearly with the viscosity contrast coefficient $\gamma$, which is not unlike the thermal convection in a pure fluid solidifying from above [17]. This linear relation is explained by the local instability concept [24] with a scale based on the convective region sitting below a stagnant lid, which is located in the region $0 \le z \le \ln \gamma$ in which, due to the large viscosity, no convection occurs. In considering the effect due to other physical parameters of the system, it is found that only $\sigma$ and $\theta_\infty$ are of significant influence on the stability criteria, and $\sigma$ is the only parameter influencing the size of the onset convection cell. These effects can be attributed to the formation of a thermal boundary layer in the fluid region, which is significantly affected by the above two parameters. Other parameters, having an effect on the morphology of the mushy layer, nevertheless, are of little influence on the stability characteristics.

All the above numerical evidence consistently indicates that the stability characteristics of the present double-diffusive convection resemble those of thermal convection. This resemblance in fact is rarely seen in the natural world. Results also show that the convection cell is of the scale of the thermal boundary layer, circulating in the melt region, while the melt in the mush does not participate in the onset of convection. This fact differs clearly from the cooling-from-below system in which the onset of plume convection (or the formation of freckles) is a direct result of the occurrence of the mush-layer-mode convection, another double-diffusive convection circulating between the melt and the mushy regions.

(For the details of the physical mechanisms corresponding to the occurrence of plumes the reader is referred to Chen et al. [13]). In the present system, since no convection occurs in the mush, the mechanism driving the occurrence of plumes does not exist and thus the system is freckle-free.

## Acknowledgements

The financial support for this work from Nation Science Council through Grants NSC 83-0401-E-002-005 and NSC 85-2212-E-002-010 is gratefully acknowledged.

## References

[1] A.F. Giamei and B.H. Kear, Met. Trans. 1 (1970) 2185.
[2] J.R. Sarazin and A. Hellawell, Met. Trans. A 15 (1988) 2163.
[3] S.M. Copley, A.F. Giamei, S.M. Johnson and M.F. Hornbecker, Met. Trans. 1 (1970) 2193.
[4] S. Tait and C. Jaupart, Nature 338 (1989) 571.
[5] C.F. Chen and F. Chen, J. Fluid Mech. 227 (1991) 567.
[6] M.H. MaCay, T.D. McCay and J.A. Hopkins, Met. Trans. B 24 (1993) 669.
[7] P. Nandapurkar, D.R. Poirier, J.C. Heinrich and S. Felicelli, Met. Trans. B 20 (1989) 711.
[8] J.C. Heinrich, S. Felicelli, P. Nandapurkar and D.R. Poirier, Met. Trans. B 20 (1989) 883.
[9] S.D. Felicelli, J.C. Heinrich and D.R. Poirier, Met. Trans. B 22 (1991) 847.
[10] A. Hellawell, J.R. Sarazin and R.S. Steube, Philos. Trans. R. Soc. London A 345 (1993) 507.
[11] M.G. Worster, J. Fluid Mech. 237 (1992) 649.
[12] G. Amberg and G.M. Homsy, J. Fluid Mech. 252 (1993) 79.
[13] F. Chen, J.W. Lu and T.L. Yang, J. Fluid Mech. 276 (1994) 163.
[14] W.-Z. Cao and D. Poulikakos, Int. J. Heat Mass Trans. 33 (1990) 427.
[15] J.S. Turner, Buoyancy Effects in Fluids (Cambridge University Press, Cambridge, 1973).
[16] D.T.J. Hurle, E. Jakeman and A.A. Wheeler, Phys. Fluids 26 (1983) 624.
[17] M.K. Smith, J. Fluid Mech. 188 (1988) 547.
[18] R.C. Kerr, A.W. Woods, M.G. Worster and H.E. Huppert, J. Fluid Mech. 216 (1990) 323.
[19] R.C. Kerr, A.W. Woods, M.G. Worster and H.E. Huppert, J. Fluid Mech. 217 (1990) 331.
[20] R.C. Kerr, A.W. Woods, M.G. Worster and H.E. Huppert, J. Fluid Mech. 218 (1990) 337.
[21] M.G. Worster, J. Fluid Mech. 167 (1986) 481.
[22] G.S. Beavers and D.D. Joseph, J. Fluid Mech. 30 (1967) 197.
[23] P.G. Baines and A.E. Gill, J. Fluid Mech. 37 (1969) 289.
[24] K.C. Stengel, D.S. Oliver and J.R. Booker, J. Fluid Mech. 120 (1982) 411.